Atmospheric
Chemistry
and Physics

Discussions

Open Access

Assessment of fire emissions inventories during the South American Biomass Burning Analysis (SAMBBA) experiment

G. Pereira[1], R. Siqueira[2], N. E. Rosário[3], K. L. Longo[2], S. R. Freitas[2], F. S. Cardozo[1], J. W. Kaiser[4], M. J. Wooster[5,6]

[1]Department of Geoscience, Federal University of Sao Joao del-Rei (UFSJ), Sao Joao del-Rei, Brazil
[2]Center for Weather Forecast and Climate Studies, National Institute for Space Research (INPE), Cachoeira Paulista, Brazil
[3]Environmental Sciences Department, São Paulo Federal University (UNIFESP), Diadema, São Paulo, Brazil
[4]Max Planck Institute for Chemistry (MPI-C), Mainz, Germany
[5]King's College London (KCL), London, United Kingdom
[6]NERC National Centre for Earth Observation (NCEO), United Kingdom

Correspondence to: G. Pereira (pereira@ufsj.edu.br)

Abstract. Fires associated with land use and land cover changes release into the atmosphere large amounts of aerosols and trace gases. Although there are several inventories of biomass burning emissions covering Brazil, there are still considerable uncertainties and differences among these. While most fire emissions inventories still utilize the parameters of vegetation fuel load, emission factors and other parameters to estimate the biomass burned and its associated emissions, certain more recent inventories tend to apply an alternative method based on fire radiative power (FRP) observations to estimate the amount of biomass burned and the corresponding emissions of trace gases and aerosols. The Brazilian Biomass Burning Emission Model (3BEM) and Fire Inventory from NCAR (FINN) are examples of the first, while Brazilian Biomass Burning Emission Model with FRP assimilation (3BEM_FRP) and Global Fire Assimilation System (GFAS) are examples of the latter method mentioned. In this paper, the output of four biomass burning emission inventories used during the South American Biomass Burning Analysis (SAMBBA) field campaign are analyzed and intercompared, focusing on eight pre-defined grids. Aerosol optical thickness derived from measurements made by the MODIS sensor operating onboard the Aqua satellite is applied to assess the inventories consistency. Significant correlation coefficients (r, p>0.05 level, Student t-test) were found between 3BEM and FINN, and between 3BEM_FRP and GFAS, with approximately 0.86 and 0.85, respectively. These results indicate that emissions estimates in this region derived via similar methods tend to agree with one other, but differ more from the estimates derived via the alternative approach. However, correlations in specific grids indicate that 3BEM and FINN typically underestimated the smoke emission loading in the eastern region of Amazon Forest, whilst 3BEM_FRP presents a tendency to overestimate fire emissions in the same area. The relationship between the 3BEM and FINN fire inventories present a correlation coefficient of 0.75-0.92, with a tendency of FINN to overestimate the emission of carbon monoxide by 20-30%. Moreover, 3BEM and GFAS shows a correlation coefficient of between 0.75-0.85, with higher values near the arc of deforestation in Amazon Rainforest. However, GFAS has a tendency to present higher carbon monoxide emissions in this region, and 3BEM_FRP tends to overestimate the emissions in soybean expansion (east of Amazon forest).

1 Introduction

Biomass burning is a global phenomenon, and an ancient practice of human occupation, as well as a natural process. It consumes large amounts of vegetation across wide areas and modifies Earth surface characteristics. Fires still nowadays play a key role in ecosystem services, opening areas for livestock and agriculture, and pest control (Shimabukuro et al., 2013). In the last five decades biomass burning has been extensively and persistently used all over the tropics for these purposes, and has been involved in widespread deforestation and forest degradation (Crutzen, 1990; Bustamante et al., 2015). Biomass burning emissions inject a considerable amount of oxidants and aerosols into the atmosphere, modifying atmospheric composition and reactivity therefore disturbing the regional climate, water and biogeochemical cycles (Andreae et al., 2002; Bowman et al., 2009). Moreover, fire emissions in tropical areas are felt not only regionally but rapidly and strongly affects the global scale due to the efficiency of the atmospheric transport processes of trace gases and aerosols emitted along with high heat release, reinforced by the intense tropical convective activity associated with high temperature and moist (Kaufman et al., 1995; Martin et al., 2010). Extensive fires activity also disturbs the environmental system, producing soil depletion, damaging flora and fauna, decreasing biodiversity, and even affecting human life (Fearnside, 2000).

An accurate temporal and spatial estimate of biomass burning emissions is critical to a reliable analysis of the associated effects, including at different time scales. Nowadays, efforts to quantify emissions from biomass burning from space-borne instruments have increased considerably in scope, but uncertainties on the input data and within the different methodologies can still lead to lead to errors of up to an order of magnitude for trace gases and aerosol emission totals (Vermote et al., 2009; Baldassarre et al., 2015). Most methodologies to estimate biomass burning emissions utilize the relationship proposed by Seiler and Crutzen (1980), usually called the "bottom-up approach":

$$M^{[\in]} = A.B.\beta.EF^{[\in]} \tag{1}$$

where $M^{[\in]}$ is the emission load of species $\in$ (g); A is the burned area (in km²); B is the fuel load (kg.km^{-2}); β is the combustion completeness (unitless); and $EF^{[\in]}$ is the emission factor released species $\in$ (g.kg^{-1}). In this method, the burned area is one of the parameters necessary to estimate the emission of trace gases and aerosols, usually estimated by Earth Observation (EO) satellites, and typically since fires must have already occurred to produce a burned area this is not that well suited to providing near real-time air quality forecasts in models that includes vegetation fires. Other factors in Equation 1 can also be difficult to determine, for example, the combustion completeness typically depends on the moisture present in the biomass (and thus in part on micrometeorology), and the fuel load (average biomass and its fraction above ground) is hardly homogeneous (Chuvieco et al., 2004; Yebra et al, 2008; De Santis et al., 2010).

In the last decade, the development of sensors more targeted at active fire observations has allowed estimation of the radiative energy flux released by fires or the fire radiative power (FRP, in J.s^{-1}). Continuous acquisition of FRP over a fires duration provides fire radiative energy (FRE, in MJ) released by the fire process. New fire emission methods utilize the FRE to calculate the amount of biomass burned and/or the emission of trace gases and aerosols (Wooster et al., 2005; Ichoku and Kaufman, 2005; Ellicot et al., 2009; Freeborn et al., 2011; Kumar et al., 2011):

$$FRE_{grid_{(lon,lat)}} = \frac{1}{2} \sum_{i=1}^{n} (FRP_n + FRP_{n+1}) \cdot (T_{n+1} - T_n) \qquad (2)$$

$$M^{[\in]} = FRE_{grid_{(lon,lat)}} \cdot \gamma \cdot EF^{[\in]} \qquad (3)$$

where $FRE_{grid_{(lon,lat)}}$ provides radiative energy at a geographical location in terms of longitude and latitude of a specific centered point of a regular grid; T is the time interval between FRP acquisitions; n represents the nth sample; and γ is the FRP-biomass conversion factor (kg.MJ^{-1}, Wooster et al., 2005; Kaiser et al., 2012). In this method, parameters such as fuel load, burning efficiency and the presence of moisture in the soil and in vegetation directly influence the observed energy radiated by the fires and do not have to be separately considered. In this way this method is sometimes referred to as a "top-down" approach.

The South American Biomass Burning Analysis (SAMBBA) was an airborne experiment design to characterize the smoke physical and chemical properties in Amazonian rainforest and central area of Brazil. The SAMBBA campaign took place in September 2012. The operational smoke forecasting system built to support SAMBBA flights planning utilized four fire emissions inventories that deployed variously the aforementioned bottom up and top down approaches: I) Brazilian Biomass Burning Emission Model (3BEM, Longo et al., 2010); II) Brazilian Biomass Burning Emission Model with FRP assimilation (3BEM_FRP, Pereira et al., 2009); III) Global Fire Assimilation System (GFAS, Kaiser et al., 2012); and IV) Fire Inventory from NCAR (FINN, Wiedinmyer et al., 2011). This study provides an intercomparison and evaluation of these inventories, with focus on the South American Biomass Burning Analysis (SAMBBA) field campaign experiment.

2 Data and methodology

2.1 Inventories description

2.1.1 Brazilian Biomass Burning Emission Models (3BEM and 3BEM_FRP)

The Brazilian Biomass Burning Emission Model (3BEM) is a model developed to estimate the daily fire emissions based on the location of actively burning fire "hotspots" (i.e. areas of combustion detected using active fire/thermal anomaly detection algorithms) derived via orbital remote sensing. The 3BEM utilizes the Wildfire Automated Biomass Burning Algorithm (WFABBA) applied in Geostationary Operational Environmental Satellite (GOES) constellation data (Prins et al., 1998); the MOD14 and MYD14 products of the Moderate Resolution Imaging Spectroradiometer (MODIS) aboard Terra and Aqua satellites (Justice et al., 2002); and the fire product developed by the Environmental Satellite Division (DSA) of National Institute for Space Research (INPE), which uses the Spinning Enhanced Visible and Infrared Imager (SEVIRI) onboard Meteosat Second Generation (MSG), GOES, MODIS and Advanced Very High Resolution Radiometer (AVHRR) onboard the National Oceanic and Atmospheric Administration (NOAA) constellation (Setzer and Pereira, 1991).

Atmospheric
Chemistry
and Physics
Discussions

The 3BEM version initially developed by Longo et al. (2010), estimates the emitted mass of trace gases and aerosols related to each fire detected by remote sensing as described in Equation 1. Therefore, the location of the detected fire hotspots are cross-tabulated with MODIS Land Cover map to allow the estimation of above-ground biomass density, combustion factor and emission factor from literature values (Olson et al., 2000; Andreae and Merlet, 2001; Houghton et al., 2001; Sestini et

5   al., 2003; Akagi et al., 2011). Also, the model filters all fires located in a 1 km radius to prevent double counting between fire products.

The updated 3BEM includes FRP assimilation (3BEM_FRP, Pereira et al., 2009), and utilizes the same algorithm of the former 3BEM but with burned biomass directly estimated using FRE estimates, as described in Equation 3. The 3BEM_FRP model groups all FRP values estimated by MODIS, GOES and METEOSAT products according to their time acquisition,

10   eliminating the low confidence fire pixels (values below 50% for MOD14, MYD14 and METEOSAT products, and flags 4 and 5 for WFABBA/GOES product) and minimizing the impact of the MODIS bow-tie effect as described in Freeborn et al. (2011).

Some of these FRP estimates are compromised by sensor saturation over larger fires, particularly GOES over South America (Xu et al., 2010). Thus, to not ignoring important episodes of biomass burning by removing GOES saturated pixels, which

15   FRP values are not provided, 3BEM_FRP utilizes Eq. (4) to estimate the energy released by fires, based on the premise that emitted spectral radiance (M_λ) in spectral band centered at 3.9 µm is proportional to FRP (Wooster et al., 2003).

$$FRP_{MIR} = \frac{Ag}{a}\sigma \int_{3.76}^{4.03} M(\lambda, T) d\lambda - M_b \qquad (4)$$

where Ag represents the area of GOES pixel (km²); a is a constant fit based in GOES MIR spectral band (W.m^{-2}.sr^{-1}.µm^{-1}.K^{-4}, Wooster et al., 2005); σ is the Stefan-Boltzmann constant (5.66 x 10^{-8} W.m^{-2}.K^{-4}); M is the Planck´s Law (W.m^{-2}.µm^{-1}); λ is

20   the wavelength (µm); T represents the temperature (K); and M_b is the radiance emitted by the background (110 MW). Also, in 3BEM_FRP methodology, FRP values estimated by GOES satellites below 1000 MW are corrected by +17% and FRP values higher than 1000 MW are corrected by +41% (Xu et al., 2010). This procedure is also applied in SEVIRI data, but due to its spatial coverage, we decided not to include this data in the present analysis. Pereira et al. (2009) describes the 3BEM_FRP method in detail.

25   A clustering process performs the combination of all detected fires from different sensors. In this step, the size of a matrix that merges FRP data can be defined according to the spatial resolution and grid configuration of the atmospheric model. Consequently, the convolution mask η(γ,κ), of size M x N (rows x columns), running over the grid with FRP areal density (defined by weighting the FRP values by pixel area) values estimated by different satellites ξ(lon,lat), will result in the grid (FRP$_{grid}$) containing all clustered fires for a given timestep.

30     $$FRP_{grid_{(lon,lat,t)}} = \sum_{\gamma=-\alpha}^{\alpha} \sum_{\kappa=-\beta}^{\beta} \eta(\gamma,\kappa)\xi(lon + \gamma, lat + \kappa, t) \qquad (5)$$

where the clustered grid is defined to all points where the mask of M x N size overlaps the image completely (lon ϵ [α, M – α], lat ϵ [β, N –β]). Moreover, if in any timestep of FRP integration the interval between two acquisitions is greater than 4

Atmospheric
Chemistry
and Physics
Discussions

hours ($\Delta T > 14400$ s), it is assumed the hypothesis of two or more independent fires, then the algorithm assumes T = 0 and another integration will be performed.

2.1.2 Global Fire Assimilation System (GFAS)

The Global Fire Assimilation System (GFAS, Kaiser et al., 2009/2012) is an approach used to map daily global fire emission
5   through FRP observations. Therefore, GFAS also assumes that the electromagnetic radiation emitted by fires is related to the consumption of burned biomass (Wooster et al., 2005). In the present GFAS version, 1.1, FRP values of MOD14 and MYD14 fire products from Terra and Aqua satellites, respectively, are used to estimate the average of observed FRP areal density (FRP_{ad}, in W.m^{-2}). GFAS estimates open vegetation fire trace gas and particulate emissions from each fire detected as described in Eq. (3).
10 The model performs a clustering process of observed FRP (F_i), pixel area (A_i) and view zenith angle (θ) to sensor pixels with valid observations (i) to estimate the FRP_{ad}. The clustering process also takes observations of F_i=0, i.e. no-fire, into account. Thus, for each individual grid cell the estimated FRP_{ad} could be calculated as:

$$FRP_{ad} = \frac{\sum_k \sum_{i_k \epsilon j} F_{i_k}. \cos^2(\theta_{i_k})}{\sum_k \sum_{i_k \epsilon j} A_{i_k}. \cos^2(\theta_{i_k})}$$

where i_k represents the pixel i of satellite product k (MOD14, MYD14). This formulation implicitly corrects the MODIS
15 bow-tie effect and partial cloud/ice/snow/water-cover of a grid cell. Observation gaps are subsequently filled with a data assimilation approach, that currently assumes persistence of the fires.

In GFAS, the coefficient that converts the FRP_{ad} to dry matter combustion rate is based on eight land cover classes, cf. Heil et al. (2010); Kaiser et al. (2012). In addition, the emission load of 40 species is calculated using emission factors from Andreae and Merlet (2001), subsequent updates and Christian et al. (2003). Kaiser et al. (2012) describes the inventories
20 method in detail.

2.1.3 Fire INventory from NCAR (FINN)

The Fire INventory from NCAR (FINN, Wiedinmyer et al., 2011) is an approach to estimate daily fire emissions at 1 km resolution through satellite observation of active fires. The FINN model produces global estimates of aerosols and trace gases of open vegetation fires, as described in Equation 1. The FINN utilizes the MOD14 and MYD14 fire products,
25 processed by MODIS Rapid Response (MRR) or by the MODIS Data Processing System (MODAPS) Collection 5. However, since MODIS observations do not cover the entire globe daily, due to orbital gaps, FINN smears MODIS detections of active fire over two days. For each fire located in the equatorial region, is assumed that in the next day the fire will be half of its original size (Wiedinmyer et al., 2011).

Similarly to 3BEM, the FINN model removes multiple detections of same fire pixel prior to estimation of the trace gases and
30 aerosols released. In addition, for each active fire, FINN estimates as 1 km² the burned area for most of land use classes, with exception to grasslands/savannas in which it is assumed the burned area as 0.75 km². To estimate the emission of trace gas

and aerosol species, emissions factors derived from Andreae and Merlet (2001) and Akagi et al. (2011) are used, as well as the MODIS land cover type for 2005 and the MODIS Vegetation Continuous Fields (VCF) product. Wiedinmyer et al. (2011) describes the procedures adopted in detail.

2.2 MODIS aerosol optical thickness

5 The aerosol optical depth (AOD) product from MODIS sensors aboard Aqua and Terra satellites platforms is used to provide a first order assessment of the impacts of the two distinct methods to estimate biomass burning emission, i.e. the bottom-up and top-down approaches. In this work, the MODIS Level 2.0 Collection 5.1 (051) data and Level 3 Atmospheric product denominated MYD08_D3 (Mean Aerosol Optical Thickness at 550 nm – AOT_{550nm}) is utilized to compare the fire emissions inventories utilized during the SAMBBA campaign between 01 Sept and 31 Oct 2012. The MODIS Atmosphere daily global

10 product estimates roughly 600 statistical datasets at 1 degree resolution and equal-angle grid that comprehends a merge of MODIS acquisition over the globe (Kaufman and Tanré, 1998). Figure 1a shows the MODIS MCD12 Land Use and Land Cover (LULC) product for South America with LULC classes described in Table 1. During the SAMBBA field campaign, the highest biomass burning aerosol loadings were observed over Brazilian territory, mainly over the southeastern edge of the Amazonian forest (dotted red line, known as Arc of Deforestation) and in the soybean expansion area in the Brazilian

15 Savannah (marked as X), as shown in the time-averaged (01 Sep 2012 – 31 Oct 2012) AOD_{550nm} field derived from MODIS sensor aboard Aqua satellite (Figure 1b). The high values of AOD related to fires located in eastern of Mato Grosso (mainly in the secondary forest) and in transition areas of Amazon rainforest and Brazilian Savannah are noteworthy; soybean expansion areas, which present high concentration of fires, have a lower amount of biomass than Amazon rainforest and the high ventilation favors the transport of smoke to west.

2.3 Inventories configuration and analysis description

To evaluate the fire emissions inventories utilized during the SAMBBA experiment, we used the 3BEM preprocessor to generate the gridded data in Geographical coordinates with a spatial resolution of 0.1°. The 3BEM preprocessor has as output daily emission load of several species, but in this work, we selected to analyze only carbon monoxide (CO) emission fields, from 1st of September to 31st of October 2012. Moreover, the four inventories are compared over eight sub-domains

25 windows with a mark of 10°x10° that typically comprehends different Brazilian states (Figure 2a) and different fire regimes and biomes (Figure 2b).

3 Results and discussion

In this section, we compare the fire emissions inventories used in near real time within atmospheric-chemistry transport models to support the SAMBBA flight planning (FINN, GFAS, 3BEM, 3BEM_FRP). Each inventory's spatial distribution

of total CO emission (10^4 kg.m^{-2}) over South America, from 1st of September to 31st of October 2012, is depicted in Figure 3, according to the respective methodologies used to estimate the emission loading.

The intercomparison shown in Figure 3 demonstrates that inventories that utilize the same (i.e. top-down or bottom-up) methodology show similar spatial patterns in CO emissions (kg.m^{-2}), not only in Amazon basin but across all of South America, but differ in their absolute values. The CO emissions estimated by the 3BEM and FINN models present higher values than 3BEM_FRP and GFAS in the regions where the main processes of forest logging and subsequent agricultural expansion (GRIDS 3, 4 and 5) occur. The highest emissions in 3BEM and FINN are located mainly in Rondonia State (GRID3) and in the border of Mato Grosso State (GRID 4), where most of the SAMBBA flights took place.

Cardozo et al. (2014) analyzed the fires pattern in Rondonia between 2000 and 2011 and identified that most fires result in relatively small "burn scars" on the landscape, with areas 20 to 80 hectares (64% of cases). In addition, only 6.5% of all burned areas in Rondonia are associated with recently deforested areas. This could indicate that 3BEM and FINN are overestimating the CO emission load due to an erroneous location of fires in areas of forest instead of livestock and permanent crops, which have lower above ground biomass. Furthermore, 3BEM_FRP and GFAS inventories do not display a similar pattern to 3BEM and FINN because their emissions are directly related to FRP, with a weaker dependency on land cover type. Thus, areas with low above ground biomass will provide low values of FRE due the observed characteristics of the fire activity, and thus low values of CO.

The spatial distribution of the emission inventories suggests that fires in the region are strongly related to deforestation activity and therefore to the general economy, with a strong trend in recent years of fires in secondary forest (Cardozo et al., 2014). In Figure 3c, higher emission loads are located in the east of Brazil (GRID 5), mainly in the Cerrado biome, a vegetal formation composed of savanna and other typically low density vegetation formations, which include trees of 15 meters height (as shown in Figure 1a). This region is now economically used, constituting a new agricultural frontier of Brazil (with more than 100 million hectares suitable for modern mechanized crop agriculture, mainly soybean). In this area, the four fire inventories differ considerably. The 'top down' inventories that use the FRP approach show much higher emission loads compared to 3BEM and FINN.

The difference in emission of CO (kg.m^{-2}) between 1st of September and 31st of October 2012 was quantified via correlation coefficient analysis (all significant at $p < 0.05$) (Figure 4). The highest correlations coefficients were found between 3BEM and FINN with 0.86, between 3BEM_FRP and GFAS with 0.85, and between GFAS and FINN with 0.84. These high correlations indicate that inventories produced using similar emissions methods tend to agree with each other. The third correlation reflects that both inventories use the same active fire observations (MODIS), albeit with different data processing. We highlight that all were significant at $p>0.05$ level, Student t-test. To analyze the measures of accuracy of regression between fire inventories we used the bootstrap technique (Efron, 1982). In this technique, a population of 1.0×10^4 reconstructs the regression and provides the parameters to create the confidence interval and error analysis of model estimation.

The regression among 3BEM and FINN models present a correlation between 0.75-0.92 with a tendency of FINN to overestimate, relative to 3BEM, the emission load of CO in 20-30%. This apparent FINN overestimation is seen in the majority of grids, with the exception of grids 2, 5 and 7 (Figure 5a). In areas where FINN emissions are lower than 3BEM emissions, vegetation is mainly composed of Brazilian Cerrado (grids 2 and 5), and by Pantanal wetlands biome and croplands/livestock (grid 7) with predominant vegetation are Savannah and grassland, however, the presence of Deciduous and Semi deciduous Forest are also found. Since, 3BEM and FINN presents similar methodology to estimate the emission load of species released by wildfires, the parameters used in Equation 1, such as above ground biomass, are likely to be associated with the relatively high estimation in CO values.

The intercomparison analysis of 3BEM and GFAS inventories shows a correlation coefficient between 0.75-0.85 with higher values over the Arc of Deforestation, in the Amazon Rainforest (Figure 1a). However, GFAS has a tendency to present higher CO emissions (by 10-20%) in grids 2 and 5, and to underestimate by 20-30% in grids 3 and 4 (Figure 5b) when compared to 3BEM. In these areas, the vegetation is dominated by the Amazon biome, along with a small area of Cerrado (located in the south of the grids), with presence of Evergreen Broadleaf forest, Tropical Degraded Forest, and Cropland/livestock areas. Moreover, the FRP-based emissions estimation method utilized by GFAS presents a considerable difference in the region of soybean expansion in grid 5.

Similar to GFAS, the relationship among 3BEM and 3BEM_FRP shows a correlation coefficient between 0.65-0.75. However, 3BEM_FRP has a tendency to overestimate the CO values by 60-85% in grid 5, and to underestimate by 10-15% in grids 3 and 4 (Figure 5c). The 3BEM_FRP model presented an elevated emission of CO in grid 5, possibly due the GOES viewing zenith angle (high viewing angles results in the erroneous values of infrared brightness and present a large pixel area, Roberts et al., 2005; Vermote et al., 2009; Peterson et al., 2013). In addition, in grid 5, cloud absence may influence in the FRP cycle occasioning an overestimation due the large number of acquisitions in high view angles. The relationship between 3BEM_FRP and GFAS shows a correlation between 0.82-0.90. Accordingly, the 3BEM_FRP model has a tendency to present higher emission load of CO than GFAS, mainly in some areas of deforestation arc and in grid 5 that could reach 100% (Figure 5d). The high values are associated with assimilation of GOES FRP in 3BEM_FRP, while GFAS utilizes only MODIS FRP data.

The fieldwork measurements acquired during the SAMBBA campaign indicate that the near-real time air smoke forecasts based on traditional inventories, such as 3BEM used by Coupled Aerosol and Tracer Transport model to the Brazilian developments on the Regional Atmospheric Modelling System (CCATT-BRAMS), typically underestimated smoke loading in the central to east region of Amazon Forest (near Mato Grosso and Tocantins States) as described in Rosario et al. (2013). In addition, the models tended to overestimate the smoke loading in the Northwest part of Rondonia (indicated in Figure 2a). However, during the SAMBBA campaign were identified lower values of CO emissions, showing an overestimation of emission load in this region. In general, all fire inventories models present a good agreement, with most regressions significant at p>0.05 level, Student t-test (Table 2, non-significant regression marked in red). The only regression that

presented low values of correlation coefficients are located in Grid 5 with values lower than 0.30. Moreover, regression between 3BEMxFINN present the highest correlation in most of the grids.

Figure 6 shows the daily emission estimates from each of the models used in SAMBBA campaign integrated over the eight grids and the Lat-Lon average values of AOT_{550nm} for 01st September 2012 to 31st October 2012. During the SAMBBA

5 campaign, the grids located in arc of deforestation and in Mato Grosso state presented the highest values of averaged AOT_{550nm}. Commonly, the 'top down' inventories that use FRP to estimate the emission of CO present a similar pattern, as do the 'bottom up' models that utilizes the relationship between the burned area, fuel load and the combustion completeness. This is evident in Figure 6a, which 3BEM_FRP and GFAS has lower values during all periods, with daily emission loads of CO between 20-500 $kg.m^{-2}$ and average value of 93 $kg.m^{-2}$. In addition, 3BEM and FINN models presented a high variability

10 during the analyzed period, with the daily estimation of CO emission load that could reach values greater than 3000 $kg.m^{-2}$. The correlation coefficient of 3BEM_FRP x GFAS and 3BEM x FINN are 0.85 and 0.76, respectively, with a tendency of GFAS and 3BEM to present higher estimation of CO emission load. In the grid1, the total emission load of CO in 3BEM and FINN to 01st September 2012 to 31st October 2012 are, respectively, 61.660 and 52.971 $kg.m^{-2}$ (Table 3), an estimation 4-10 times more than GFAS and 3BEM_FRP.

15 Figure 6b shows the time series of CO and AOT_{550nm} in grid2, with the four models presented showing similar patterns with high emission values on 09th September 2012 and between 20th-30th October 2012. The correlation coefficient of 3BEM_FRP x GFAS and 3BEM x FINN are 0.78 and 0.75 with a tendency of 3BEM (55.234 $kg.m^{-2}$) and 3BEM_FRP (29.059 $kg.m^{-2}$) to present higher estimation of CO emission load in this region. Also, we could observe a good agreement between CO emission load estimated by the four models and MODIS AOT_{550nm}. However, the grid3 presented distinct CO

20 distributions to the four models (Figure 6c). In September, FINN and 3BEM presented highest values when compared with 3BEM_FRP and GFAS during all period. However, 3BEM_FRP shows higher values than GFAS in September and otherwise in October. The correlation coefficient of 3BEM_FRPxGFAS and 3BEMxFINN are 0.87 and 0.94, respectively, with a tendency of FINN and 3BEM_FRP to present higher estimation of CO emission load. The relationship between GFASxFINN presents a correlation coefficient of 0.91. However, the total emission load of CO estimated by FINN (163.552

25 $kg.m^{-2}$) is 3 times more than GFAS (54.891 $kg.m^{-2}$).

In Grid4, all inventories showed a good agreement with correlations coefficients greater than 0.90. However, during the period from 3rd of September to 10th of September, 3BEM_FRP presented six episodes with higher emission loads, undetected in the other inventories (Figure 6d). The outlier values in 3BEM_FRP are likely to be related to GOES FRP acquisitions, which suggests inconsistencies in GOES data acquisition due to viewing angle and errors in data processing.

30 The grid5 presented the lowest correlation coefficient between 3BEM and FINN models during the SAMBBA campaign with 0.30. In this grid, FINN presents a low estimation of CO emission load when compared with the other models (as demonstrate in Table 3). In this region, FRP methods showed more emission than the bottom up methods. The 3BEM_FRP model overestimated in more than 100% the emission values compared to GFAS (Figure 6e), however, the correlation between these models is 0.84. In the other grids, the fire-related emission of CO provided by the four models show a

considerable consistency, with few differences in absolute values, indicating a good agreement across these other regions of South America (Figures 6f-6h).

During the SAMBBA campaign, operational atmospheric chemistry transport models were applied in real time: I) the Monitoring Atmospheric Composition and Climate (MACC) from European Centre for Medium-Range Weather Forecasts
5   (ECMWF) with GFAS; and II) CCATT-BRAMS with 3BEM. Figure 7 shows the simulated AOT_{550nm} from MACC/ECMWF (red line), CCATT-BRAMS (blue line), and estimated by Terra (green line) and Aqua (black line) to the eight grids. Although 3BEM present the highest emission load in Grid1 and Grid2, the CCATT-BRAMS simulation underestimate the MODIS AOT_{550nm}. In these grids, the MACC/ECMWF model presents a better consistency with the satellite measurements. One potential reason for the underestimation of CCATT-BRAMS is related to background aerosol
10   unrelated to the fires directly being observed and that is not included in this model, causing low values of simulated AOT_{550nm} for these grids. Also, MACC/ECMWF assimilates MODIS aerosol optical depth observations, and even with low CO emission values in Grids 1 and 2 the aerosol simulation present a good agreement with observation data.

The assessment of MACC/ECMWF and CCATT-BRAMS models against MODIS AOT_{550mm} reveals a good agreement in terms of the general pattern of the temporal evolution. As shown in the AOT_{550mm} time series, both methods appear to be able
15   to estimate the influence of aerosols released by fires rather well. However, when the intensity of the biomass burning is too high, the values simulated by MACC/ECMWF and CCATT-BRAMS for the grids 4-8 appear underestimated, possibly due to the influence of smoke on the FRP measurements, lack of fire observations, clouds, above ground biomass data and fire size. Moreover, it is possibly to identify an overestimation in Grid3, mainly due to out of date land use and land cover map that insert fires over forest areas even if the area was burned/deforested in past years, and a very noticeable underestimation
20   in Grid5, as demonstrated in the inventories.

4 Conclusions

Full characterization of the emissions of trace gases and aerosols are often essential for assessing the atmospheric impacts of fire and for constructing fire inventories. These inventories generally rely on data from environmental satellites, and provide useful information for weather, climate and air quality models. In this study, we analyzed data from the four biomass burning
25   emissions inventories used during the SAMBBA airborne atmospheric sampling and remote sensing campaign that took place in Rondoni (Brazil) between 1 September 2012 and 31 October 2012. Each inventory utilizes distinct methodology, with 3BEM and FINN deriving the emission of trace gases and aerosols through a 'bottom up' combination of burned area and fuel load metrics based on vegetation maps and field-location specific coefficients, whilst 3BEM_FRP and GFAS estimate biomass burned more directly from 'top down' FRP measurements made by the EO satellite instruments.
30   The evaluation of the emissions models focused on eight pre-defined grids, (Figure 2) and demonstrates that inventories that utilize the same methodology, such as 3BEM and FINN on the one hand ('bottom up') and GFAS and 3BEM_FRP on the other ('top down'), show similar patterns in emission spatial distribution, not only in the deforestation arc but also throughout

South America. However they can differ in their absolute values. As such, each inventory particular characteristics, with 3BEM and FINN showed higher emissions of CO values in the Amazon forest logging area, where most of the SAMBBA campaign flights occurred. Furthermore, these models typically underestimated the smoke loading in the southeast region of Amazon Forest and in the northwest of Rondonia, where 3BEM_FRP and GFAS deliver a better accuracy. The best overall correlations coefficients were found between 3BEM and FINN, with approximately 0.86 and 3BEM_FRP and GFAS, with approximately 0.85, which indicate that similar emissions methods tend to agree with each other.

During the SAMBBA campaign, the assessment of simulated AOT_{550nm} from MACC/ECMWF and CCATT-BRAMS operational atmospheric chemistry transport models with MODIS AOT_{550nm} Terra and Aqua measurements show a good agreement related with general pattern of the time-series. Also, MACC/ECMWF and CCATT-BRAMS models are capable to simulate the aerosols released by fires. However, when the intensity of the biomass burning is too high, the aerosol values simulated by the two models underestimates the MODIS measurements. Furthermore, the evaluation between the 3BEM and FINN fire inventories present a correlation coefficient between 0.75-0.92, with total emission of CO estimated by FINN greater than 3BEM in grids 3,4,6 and8. Moreover, 3BEM_FRP and GFAS shows a correlation coefficient of between 0.65-0.95, with total emission of CO estimated by GFAS greater than 3BEM_FRP in grids 1, 6 and 8.

5 Acknowledgements

6 References

Akagi, S. K., Yokelson, R. J., Wiedinmyer, C., Alvarado, M. J., Reid, J. S., Karl, T., Crounse, J. D., and Wennberg, P. O.: Emission factors for open and domestic biomass burning for use in atmospheric models, Atmos. Chem. Phys., 11, 4039–4072, doi:10.5194/acp-11-4039-2011, 2011.

Andreae, M. O. and Merlet, P.: Emission of trace gases and aerosols from biomass burning, Global Biogeochem. Cy., 15, 955–966, 2001.

Baldassarre, G., Pozzoli, L., Schmidt, C. C., Unal, A., Kindap, T., Menzel, W. P., Whitburn, S., Coheur, P.F., Kavgaci, A., and Kaiser, J. W.: Using SEVIRI fire observations to drive smoke plumes in the CMAQ air quality model: a case study over Antalya in 2008, Atmos. Chem. Phys., 15, 8539–8558, doi:10.5194/acp-15-8539-2015, 2015.

Bowman, D. M. J. S., Balch, J. K., Artaxo, P., Bond, W. J., Carlson, J. M., Cochrane, M. A., D'Antonio, C. M., DeFries, R. S., Doyle, J. C., Harrison, S. P., Johnston, F. H., Keeley, J. E., Krawchuk, M. A., Kull, C. A., Marston, J. B., Moritz, M. A., Prentice, I. C., Roos, C. I., Scott, A. C., Swetnam, T. W., van der Werf, G. R., and Pyne, S. J.: Fire in the Earth System, Science, 324, 481-484, 2009.

Atmospheric
Chemistry
and Physics
Discussions

Bustamante, M. M. C., Roitman, I., Aide, T. M., Alencar, A., Anderson, L., Aragão, L., Asner, G. P., Barlow, J., Berenguer, E., Chambers, J., Costa, M. H., Fanin, T., Ferreira, L. G., Ferreira, J. N., Keller, M., Magnusson, W. E., Morales, L., Morton, D., Ometto, J. P. H. B., Palace, M., Peres, C., Silvério, D., Trumbore, S., and Vieira, I. C. G.: Towards an integrated monitoring framework to assess the effects of tropical forest degradation and recovery on carbon stocks and biodiversity, Glob. Change Biol., 1, 2015.

Cardozo, F. S., Pereira, G., Shimabukuro, Y. E., and Moraes, E. C.: Analysis and Assessment of the Spatial and Temporal Distribution of Burned Areas in the Amazon Forest, Remote Sens., 6, 8002-8025, 2014.

Chuvieco, E., Cocero, D., Riano, D., Martinc, P., Martínez-Vegac, J., Rivad, J., and Pérez, F.: Combining NDVI and surface temperature for the estimation of live fuel moisture content in forest fire danger rating, Remote Sensing of Environment, 92, 322–331, 2004.

Christian, T. J., Kleiss, B., Yokelson, R. J., Holzinger, R., Crutzen, P. J., Hao, W. M., Saharjo, B. H., and Ward, D. E.: Comprehensive laboratory measurements of biomass-burning emissions: 1. Emissions from Indonesian, African, and other fuels, J. Geophys. Res, 108, 4719, doi:10.1029/2003JD003704, 2003.

De Santis, A., Asner, G. P., Vaughan, P. J., and Knapp, D. E.: Mapping burn severity and burning efficiency in California using simulation models and Landsat imagery, Remote Sens. Environ., 114, 1535-1545, doi: 10.1016/j.rse.2010.02.008, 2010.

Efron, B.: The jackknife, the bootstrap, and other resampling plans. Society of Industrial and Applied Mathematics, CBMS-NSF Monographs, 38, 1982.

Ellicott, E., Vermote, E., Giglio, L., and Roberts, G.: Estimating biomass consumed from fire using MODIS FRE, Geophys. Res. Lett., 36, 2009.

Fearnside, P. M.: Global warming and tropical land use change: Greenhouse gas emissions from biomass burning, decomposition and soils in forest conversion, shifting cultivation and secondary vegetation, Climatic Change, 46, 115–158, 2000.

Freeborn, P. H., M. J. Wooster, and Roberts, G.: Addressing the spatiotemporal sampling design of MODIS to provide estimates of the fire radiative energy emitted from Africa, Remote Sens. Environ, 115, 475–498, 2011.

Heil, A., Kaiser, J. W., van der Werf, G. R., Wooster, M. J., Schultz, M. G., and Dernier van der Gon, H.: Assessment of the real-time fire emissions (GFASv0) by MACC, Tech. Memo. 628, ECMWF, Reading, UK, 2010.

Houghton, R. A., Lawrence, K. T., Hackler, J. L., and Brown, S.: The spatial distribution of forest biomass in the Brazilian Amazon: A comparison of estimates, Glob. Change Biol., 7, 731–746, 2001.

Ichoku, C. and Kaufman, Y. J.: A method to derive smoke emission rates from MODIS fire radiative energy measurements, IEEE TGRS, 43, 2636–2649, 2005.

Justice, C. O., Giglio, B., Korontzi, S., Owens, J., Morisette, J. T., Roy, D. P., Descloitres, J., Alleaume, S., Petitcolin, F., and Kaufman, Y.: The MODIS fire products, Remote Sens. Environ, 83, 244-262, 2002.

Kaiser, J. W., Suttie, M., Flemming, J., Morcrette, J.-J., Boucher, O., and Schultz, M. G.: Global real-time fire emission estimates based on space-borne fire radiative power observations, AIP Conf. Proc., 1100, 645–648, 2009.

Kaiser, J. W., Heil, A., Andreae, M. O., Benedetti1, A., Chubarova, N., Jones, L., Morcrette, J.-J., Razinger, M., Schultz, M. G., Suttie, M., and van der Werf, G. R.: Biomass burning emissions estimated with a global fire assimilation system based on observed fire radiative power, Biogeosciences, 9, 527–554, 2012.

Kaufman, Y. J. and Tanre, D.: Algorithm for Remote Sensing of Tropospheric Aerosols from MODIS, MODIS Algorithm Theoretical Basis Document. Product ID: MOD04, Revised 26 October, 1998. Available at: <http://modis.gsfc.nasa.gov/data/atbd/atbd_mod02.pdf>.

Kaufman, J. B., Cummings, D. L., Ward, D. E., Babbitt, R.: Fire in the Brazilian Amazon: Biomass, nutrient pools, and losses in slashed primary forests, Oecologia, 104, 397–408, 1995.

Longo, K., Freitas, S. R., Setzer, A., Prins, E., Artaxo, P., and Andreae, M.: The Coupled Aerosol and Tracer Transport model to the Brazilian developments on the Regional Atmospheric Modeling System (CATT-BRAMS), Part 2: Model sensitivity to the biomass burning inventories, Atmos. Chem. Phys. Dis., 7, 8571-8595, 2007.

Longo, K. M., Freitas, S. R., and Andreae, M. O.: The Coupled Aerosol and Tracer Transport model to the Brazilian developments on the Regional Atmospheric Modeling System (CATT-BRAMS). Part 2: Model sensitivity to the biomass burning inventories, Atmos. Chem. Phys., 10, 5785–5795, 2010.

Kumar S. S., Roy D. P., Boschetti L., and Kremens R.: Exploiting the power law distribution properties of satellite fire radiative power retrievals: A method to estimate fire radiative energy and biomass burned from sparse satellite observations, J. Geophys. Res., 116, doi:10.1029/2011JD015676, 2011.

Olson, J. S., Watts, J. A., and Allison, L. J.: Major world ecosystem complexes ranked by carbon in live vegetation: A database. Available from: http://cdiac. esd.ornl.gov/ndps/ndp017.html [Accessed August 7, 2010], 2000.

Peterson, D., Wang, J., Ichoku, C., Hyer, E., and Ambrosia, V.: A sub-pixel-based calculation of fire radiative power from MODIS observations: 1: Algorithm development and initial assessment, Remote Sens. Environ, 129, 262-279, doi: 10.1016/j.rse.2012.10.036, 2012.

Roberts, G., Wooster, M. J., Perry, G. L. W., Drake, N., Rebelo, L. M., and Dipotso, F.: Retrieval of biomass combustion rates and totals from fire radiative power observations: Application to southern Africa using geostationary SEVIRI imagery, J. Geophys. Res-Atmos., 110, 2005.

Rosário, N. E., Longo, K. M., Freitas, S. R., Yamasoe, M. A., and Fonseca, R. M. Modeling the South American regional smoke plume: aerosol optical depth variability and surface shortwave flux perturbation, Atmos. Chem. Phys., 13,2923-2938, 2013.

Seiler, W. and Crutzen, P. J.: Estimates of gross and net fluxes of carbon between the biosphere and atmosphere from biomass burning, Clim. Change, 2, 207–247, 1980.

Sestini, M., Reimer, E., Valeriano, D., Alvalá, R., Mello, E., Chan, C., and Nobre, C.: Mapa de cobertura da terra da Amazônia legal para uso em modelos meteorológicos. In: Simpósio Brasileiro de Sensoriamento Remoto (SBSR), 11., Belo Horizonte. Anais ... São José dos Campos: INPE, 2003. Artigos, p. 2901–2906. CD-ROM, On-line. ISBN 85-17-00018-8

Setzer, A. W., Pereira Jr, A. C., and Pereira, M.C.: Satellite studies of biomass burning in Amazonia: some practical aspects,

5   Remote Sensing Reviews, 10, 91-103, 1994.

Shimabukuro, Y. E., Pereira, G.; Cardozo, F. S., Stockler, R., Freitas, S. R., and Coura, S. M. C.: Biomass burning emission estimation in Amazon tropical forest. In: Domingo Alcaraz Segura; Carlos Marcelo Di Bella; Julieta Veronica Straschnoy. (Org.). Earth Observation of Ecosystem Services. 1ed.Oxford, UK: Taylor & Francis, 1, 112-130, 2013.

Val Martin, M., Logan, J. A., Kahn, R. A., Leung, F.-Y., Nelson, D. L., and Diner, D. J.: Smoke injection heights from fires

10   in North America: analysis of 5 years of satellite observations, Atmos. Chem. Phys., 10, 1491–1510, doi:10.5194/acp-10-1491- 2010, 2010.

Pereira, G., Freitas, S. R., Moraes, E. C., Ferreira, N. J., Shimabukuro, Y. E., Rao, V. B., and Longo, K. M.: Estimating trace gas and aerosol emissions over South America: Relationship between fire radiative energy released and aerosol optical depth observations, Atmos. Environ., 43, 6388–6397, 2009.

15   Prins, E. M. and Menzel, W. P.: Geostationary satellite detection of biomass burning in South America, Int. J. Remote Sens., 13, 2783–2799, 1992

Vermote, E., Ellicott, E., Dubovik, O., Lapyonok, T., Chin, M., Giglio, L., and Roberts, G. J.: An approach to estimate global biomass burning emissions of organic and black carbon from MODIS fire radiative power, J. Geophys. Res., 114, 205–227, 2009.

20   Wiedinmyer, C., Akagi, S. K., Yokelson, R. J., Emmons, L. K., Al-Saadi, J. A., Orlando, J. J., and Soja, A. J.: The Fire INventory from NCAR (FINN): a high resolution global model to estimate the emissions from open burning, Geosci. Model Dev., 4, 625–641, 2011.

Wooster, M. J., Zhukov, B., and Oertel, D.: Fire radiative energy for quantitative study of biomass burning: Derivation from the BIRD experimental satellite and comparison to MODIS fire products, Remote Sens. Environ, 86, 83–107, 2003.

25   Wooster, M. J., Roberts, G., and Perry, G. L. W.: Retrieval of biomass combustion rates and totals from fire radiative power observations: Calibration relationships between biomass consumption and fire radiative energy release, J. Geophys. Res., 110, D24311, 2005.

Xu, W., Wooster, M., Roberts, G., and Freeborn, P.: New GOES imager algorithms for cloud and active fire detection and fire radiative power assessment across North, South and Central America, Remote Sens. Environ., 114, 1876–1895, 2010.

30   Yebra, M., Chuvieco, E. and Riano, D.: Estimation of live fuel moisture content from MODIS images for fire risk assessment, Agr. Forest Meteorol., 148, 523–536, 2009.

Table 1. LULC classes based on Global Land Cover Characterization (GLCC).

1	Crop / Mixed farming	11	Semi-desert
2	Short grassland	12	Ice cap/glacier
3	Evergreen needleleaf tree	13	Bog or marsh
4	Deciduous needleleaf tree	14	Inland water
5	Deciduous broadleaf tree	15	Ocean
6	Evergreen broadleaf tree	16	Evergreen shrub
7	Tall grass	17	Deciduous shrub
8	Desert	18	Mixed Woodland
9	Tundra	19	Forest/Field mosaic
10	Irrigated Crop	20	Water and Land mixture

Table 2. Correlation coefficients (r) between 3BEM, 3BEM_FRP, FINN and GFAS emission inventories to the eight grids.

	3BEM_FRP	FINN	GFAS
3BEM_G1	0.84	0.85	0.82
3BEM_FRP_G1		0.67	0.76
FINN_G1			0.82
3BEM_G2	0.70	0.75	0.79
3BEM_FRP_G2		0.61	0.78
FINN_G2			0.82
3BEM_G3	0.78	0.94	0.90
3BEM_FRP_G3		0.77	0.87
FINN_G3			0.91

3BEM_G4	0.81	0.93	0.90
3BEM_FRP_G4		0.71	0.90
FINN_G4			0.88
3BEM_G5	**0.16**	0.30	0.36
3BEM_FRP_G5		0.47	0.84
FINN_G5			0.80
3BEM_G6	0.46	0.89	0.88
3BEM_FRP_G6		0.32	0.65
FINN_G6			0.81
3BEM_G7	0.68	0.89	0.85
3BEM_FRP_G7		0.60	0.79
FINN_G7			0.85
3BEM_G8	0.63	0.84	0.79
3BEM_FRP_G8		0.65	0.65
FINN_G8			0.91

Table 3. Total mean emissions (kg.m^{-2}) of CO in the eight grids shown in Figure 2.

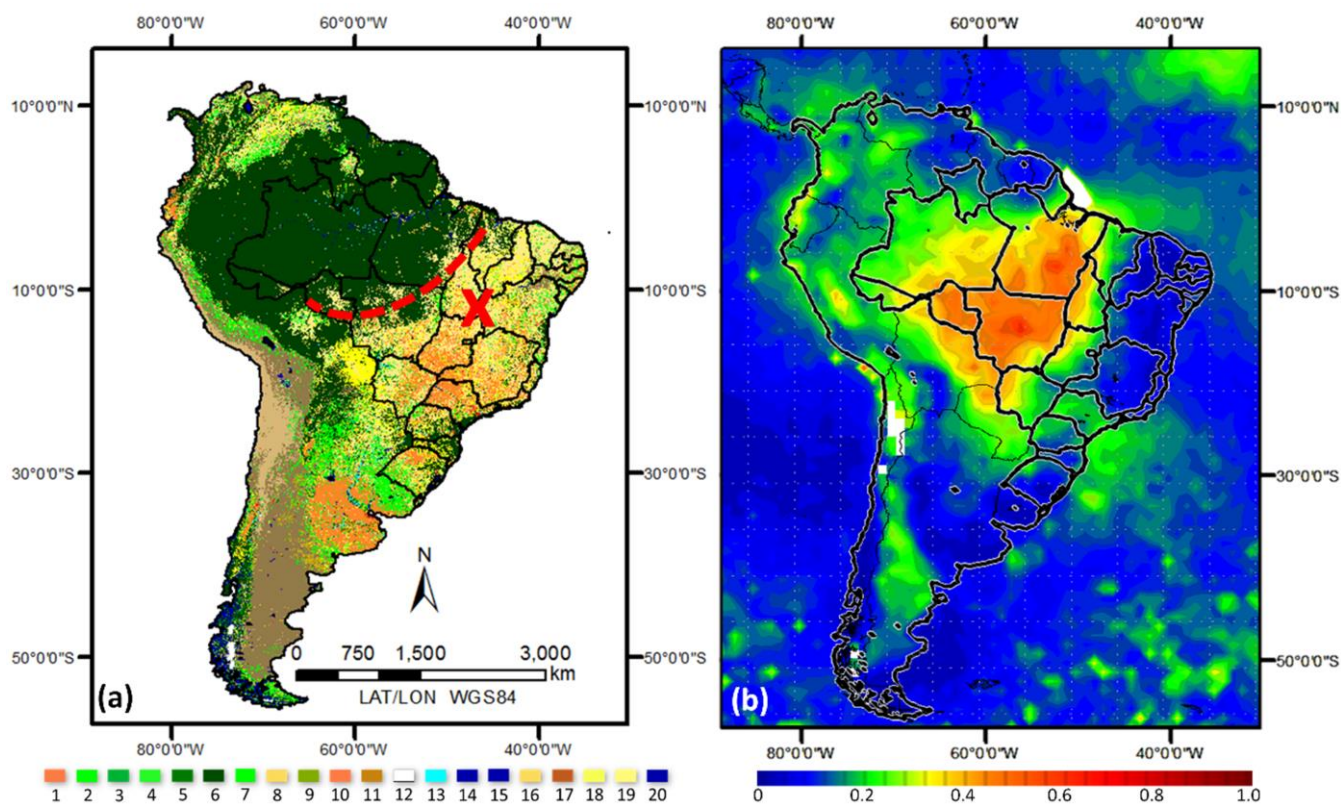|	Total Emission of CO (kg.m^{-2})			
	3BEM	**FINN**	**GFAS**	**3BEM_FRP**
GRID1	61.660	52.971	17.485	5.636
GRID2	55.234	42.631	27.706	29.059
GRID3	155.346	163.552	54.891	56.815
GRID4	151.720	167.518	91.905	166.423
GRID5	82.271	45.945	129.866	274.896
GRID6	35.199	40.412	31.118	29.811
GRID7	53.072	28.266	43.981	48.541
GRID8	11.342	13.252	25.674	19.633
TOTAL	605.844	554.547	422.626	630.814

Figure 1. (a) MCD12 Land Use and Land Cover (LULC) for South America with dotted red line representing the Amazonian Arc of Deforestation and soybean expansion in Brazilian Cerrado (marked as X); (b) Time-averaged Aqua MODIS aerosol optical thickness at 550 nm during 01 Sep 2012 – 31 Oct 2012 over South America.
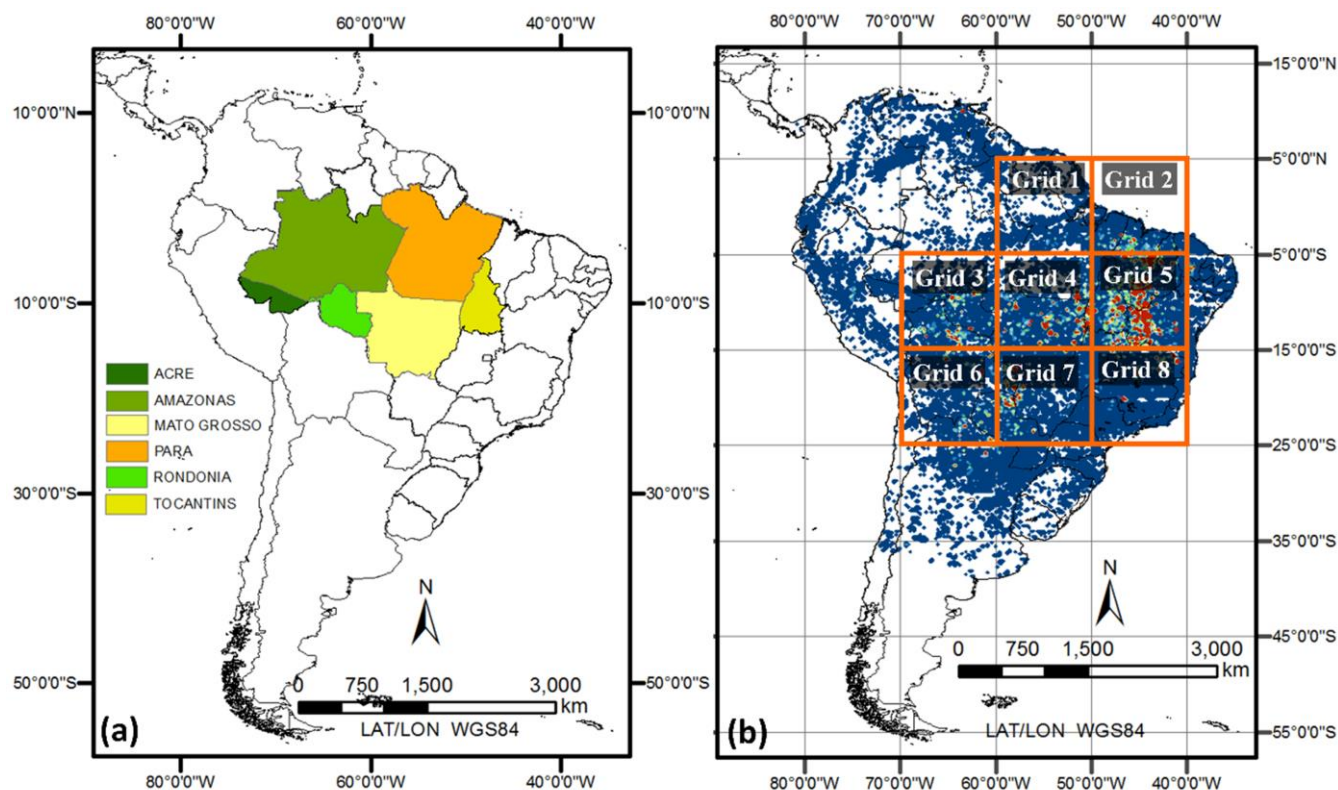
5

Figure 2. South America maps highlighting (a) the Brazilian states of Acre, Amazonas, Mato Grosso, Para, Rondonia and Tocantins, where SAMBBA field campaign took place; and (b) the eight sub-domains windows for the biomass burning inventories comparison.

5

10
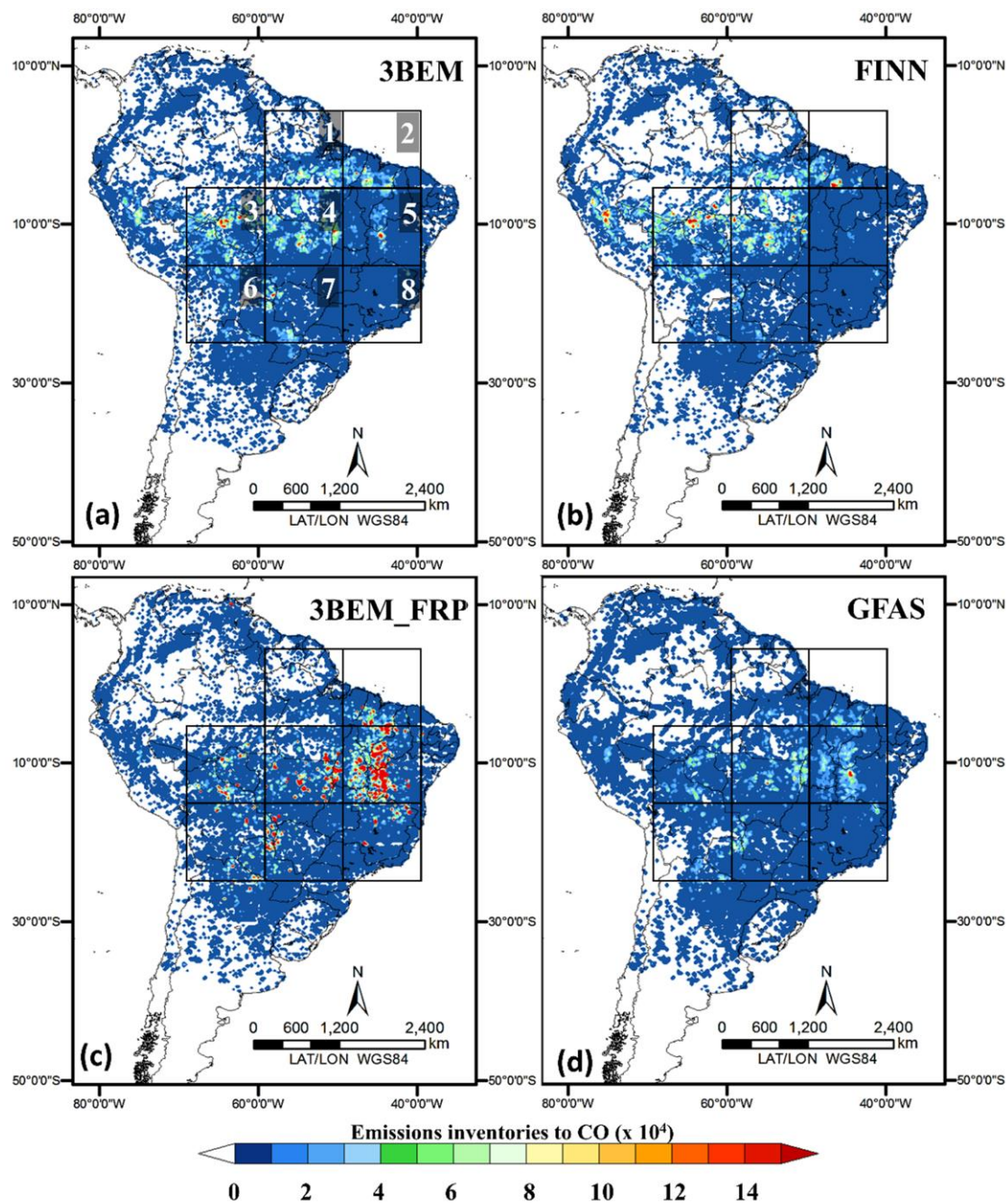
Figure 3. Spatial distribution of total CO emissions (10^4 kg.m^{-2}) over South America from 1st September to 31st of October 2012, estimated by (a) 3BEM, (b) FINN, (c) 3BEM_FRP , and (d) GFAS.
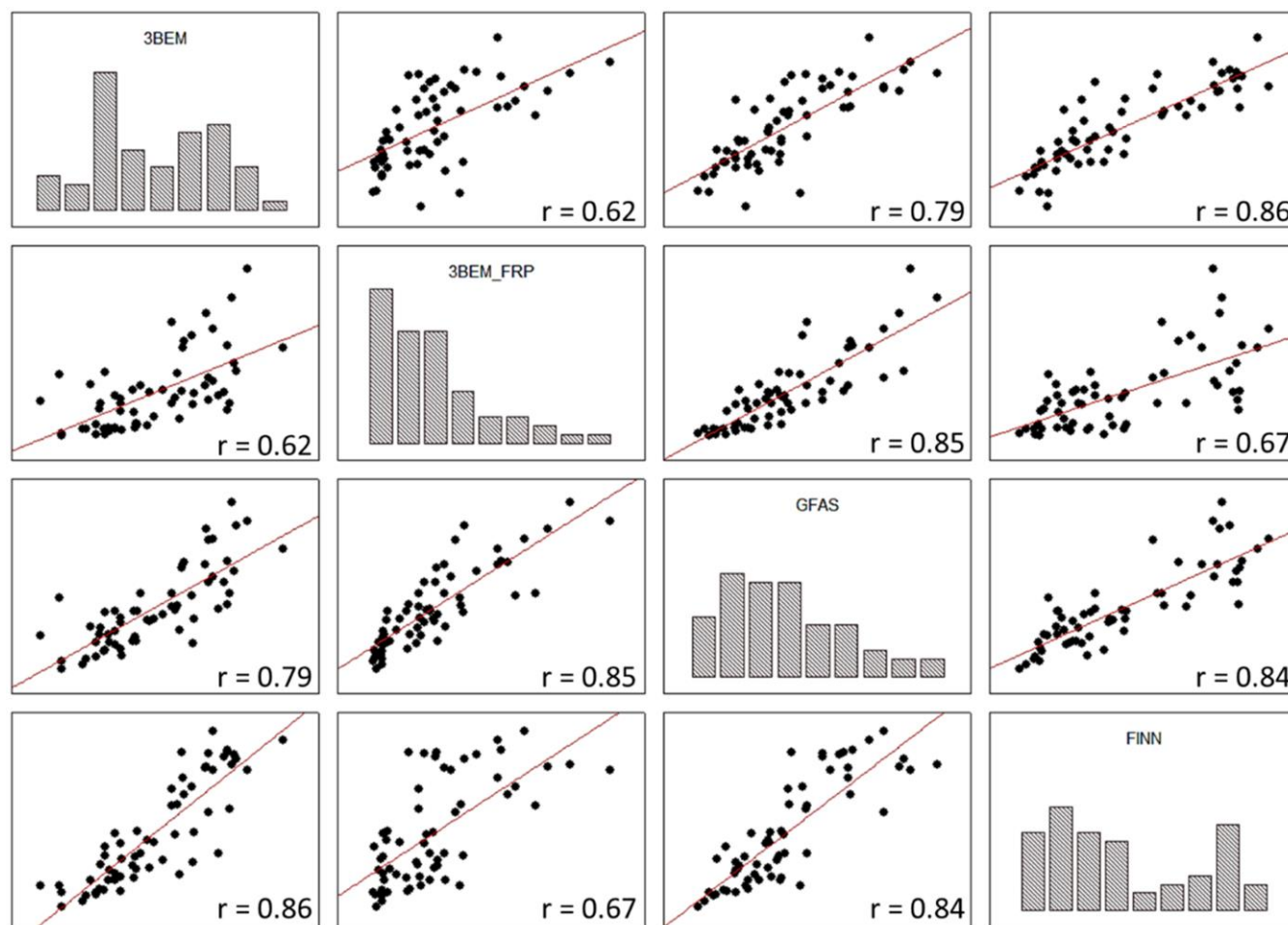
Figure 4. Linear regression between daily emission load of CO from 3BEM, 3BEM_FRP, FINN and GFAS examined
between 1st September to 31st of October 2012. In the graph, x and y-axis represent the CO (kg.m^{-2}) of each fire inventory
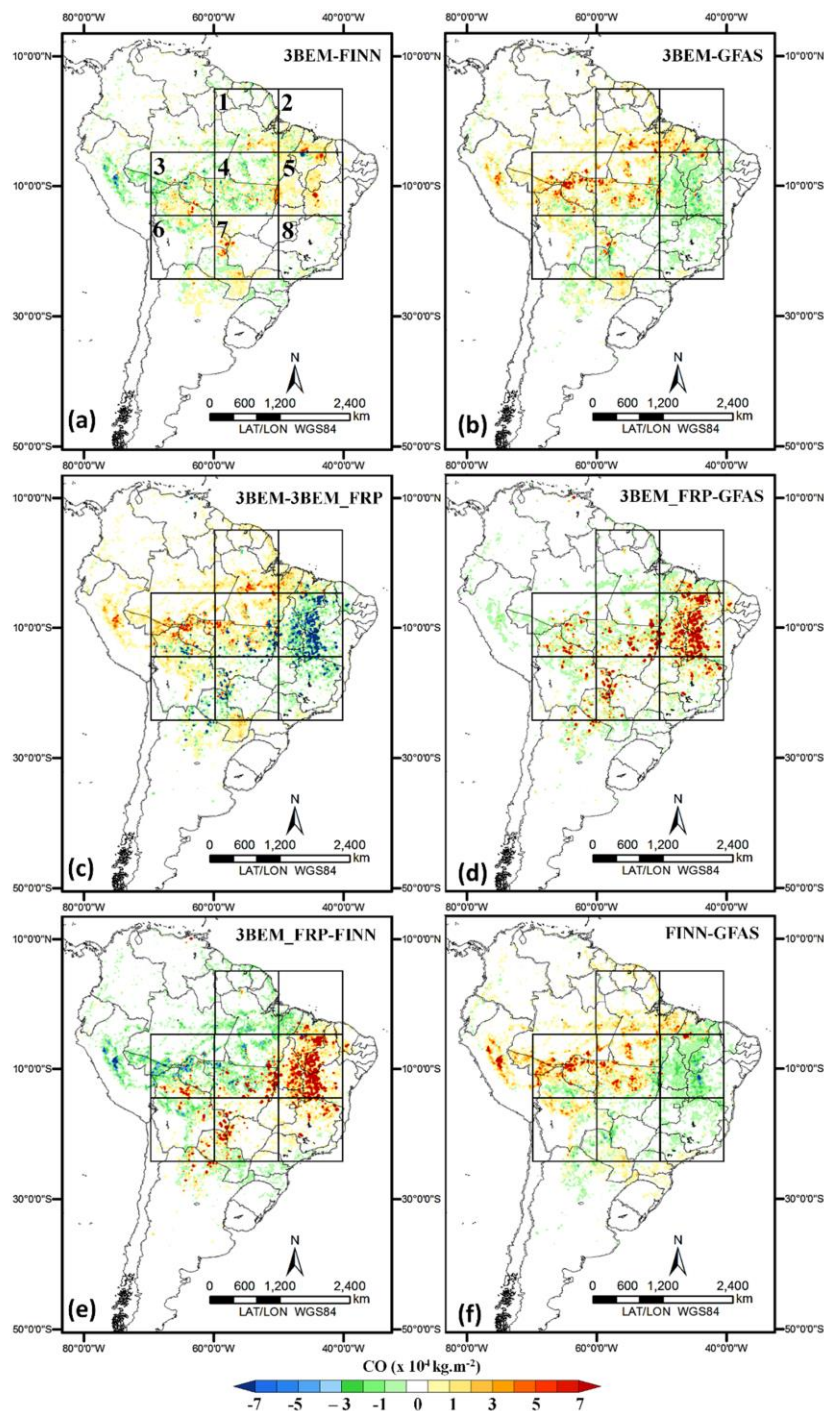(i.e. the first line of 3BEM regressions, 3BEM_FRP, GFAS and FINN are x-axis).

10

Atmospheric
Chemistry
and Physics
Discussions

Figure 5. Difference between fire inventories. A) 3BEM-FINN; B) 3BEM-GFAS; C) 3BEM-3BEM_FRP; d) 3BEM_FRP-GFAS; e) 3BEM_FRP-FINN; f) FINN-GFAS.
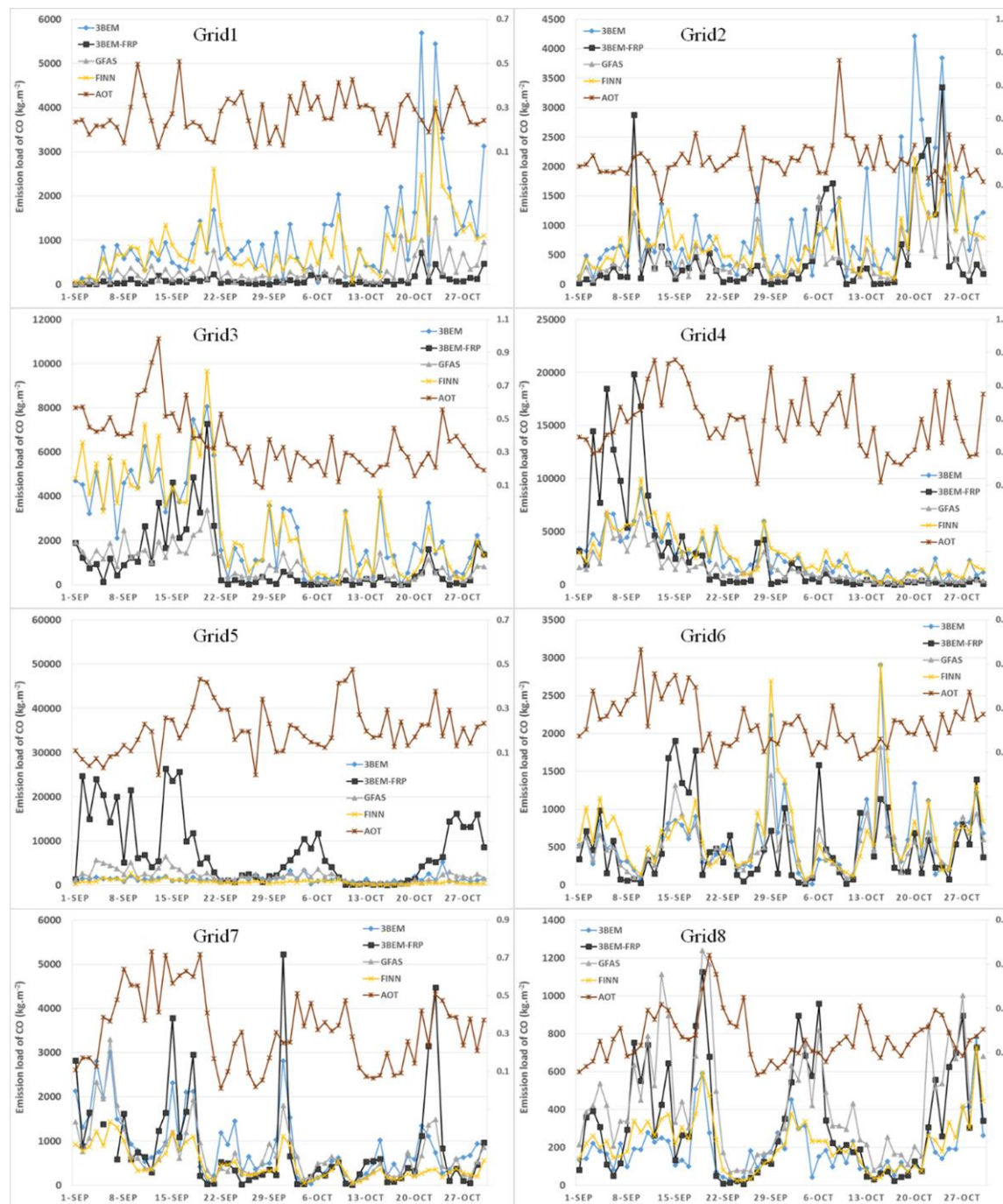
Figure 6. Lat-Lon Average time series of Aqua MODIS AOT$_{550nm}$ and 3BEM, 3BEM_FRP , GFAS, and FINN emission load of CO time series.

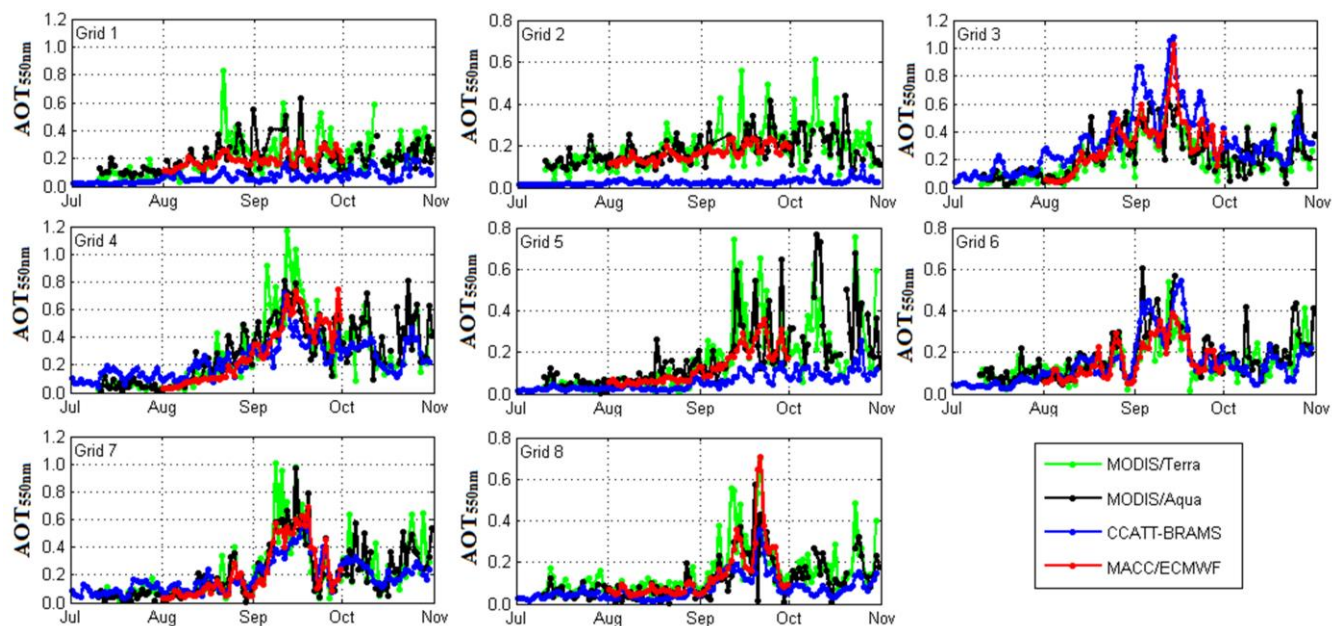Atmospheric
Chemistry
and Physics
Discussions

Figure 7. Lat-Lon Average time series of Terra/MODIS AOT_{550nm} (in green), Aqua/MODIS AOT_{550nm} (in black), CCATT-BRAMS simulated AOT_{550nm} (in blue) and MACC/ECMWF (in red) AOT_{550nm} analysis. Grids are those show in Figure 2.

5